


Article

Heavy Mineral Assemblage Variation in Late Cenozoic Sediments from the Middle Yangtze River Basin: Insights into Basin Sediment Provenance and Evolution of the Three Gorges Valley

Chunguo Kang ^{1,*}, Chang'an Li ², Chuanyi Wei ³ , Yufen Zhang ⁴, Huajun Jiang ⁵, Yawei Li ² and Rujun Guo ⁶¹ School of Geography and Tourism, Harbin University, Harbin 150086, China² School of Geography and Information Engineering, China University of Geosciences, Wuhan 430074, China; chanli@cug.edu.cn (C.L.); liyawei@cug.edu.cn (Y.L.)³ State Key Laboratory of Earthquake Dynamics, Institute of Geology, China Earthquake Administration, Beijing 100029, China; chuanyiwei@ies.ac.cn⁴ Institute of Geophysics and Geomatics, China University of Geosciences, Wuhan 430074, China; zhyfcug@163.com⁵ College of Education Science, Hunan First Normal University, Changsha 410205, China; jkyjhj@hnfnu.edu.cn⁶ School of Earth Sciences, China University of Geosciences, Wuhan 430074, China; rujunguogeology@gmail.com

* Correspondence: chunguokang@sohu.com



check for updates

Citation: Kang, C.; Li, C.; Wei, C.; Zhang, Y.; Jiang, H.; Li, Y.; Guo, R. Heavy Mineral Assemblage Variation in Late Cenozoic Sediments from the Middle Yangtze River Basin: Insights into Basin Sediment Provenance and Evolution of the Three Gorges Valley. *Minerals* **2021**, *11*, 1056. <https://doi.org/10.3390/min11101056>

Academic Editors: David Gómez-Gras and Marta Roigé

Received: 18 August 2021

Accepted: 23 September 2021

Published: 28 September 2021

Publisher's Note: MDPI stays neutral with regard to jurisdictional claims in published maps and institutional affiliations.

Abstract: The Three Gorges valley is one of the two key capture points of the evolution of the Yangtze River, yet the formation of this valley—from the pre-Miocene to the late Pleistocene—remains uncertain. The Jiangnan Basin, a late Mesozoic–Cenozoic basin located just downstream of the Three Gorges valley, is a crucial area for understanding the formation of the valley. In this study, we used heavy mineral assemblages to trace the provenance of Pliocene–Pleistocene sediments obtained from the 300-m-depth Zhoukao drillcore in the Jiangnan Basin. Results show that heavy mineral concentrations, compositions, and species display a clear change at a depth of 110 m in the studied core, consistent with the change in values of magnetic indexes and trace-element geochemical indicators. The heavy mineral assemblage deposited below a depth of 110 m (lower section of the core) comprises zircon, epidote, leucosene, rutile, anatase, pyrite, and titanite, whereas that deposited above 110 m (upper section) consists of hornblende, pyroxene, garnet, hematite-limonite, and magnetite. In addition, the heavy mineral assemblage of the upper section is similar to that of the modern surface fluvial sediments of the Yangtze, which indicates that materials of the upper core section of the Jiangnan Basin were sourced from the upper Yangtze River Basin, west of the Three Gorges. After incision of the Three Gorges valley, sediments from the upper Yangtze were transported to the Jiangnan Basin and deposited. Combining the results of this study with the known paleomagnetic chronology of the Jiangnan Basin, we propose that the Three Gorges valley was incised at ca. 1.1 Ma.

Keywords: heavy mineral; late Cenozoic sediment; Jiangnan Plain; Three Gorges; Yangtze River



Copyright: © 2021 by the authors. Licensee MDPI, Basel, Switzerland. This article is an open access article distributed under the terms and conditions of the Creative Commons Attribution (CC BY) license (<https://creativecommons.org/licenses/by/4.0/>).

1. Introduction

As the largest fluvial system draining the Tibet Plateau, the Yangtze River delivers large amounts of sediment from its headwater regions to the middle–lower reaches and the adjacent East China Sea [1–7] (Figure 1a,b). Chronological data and provenance interpretations of these ancient Yangtze sediments have helped not only to understand the temporal and spatial variation in sediment source-to-sink processes but also to reconstruct the evolution of the Yangtze River [8–12]. Recognition of the source-to-sink delivery pattern of Yangtze River sediments has allowed a better understanding to be gained of the processes

involved in the transportation of vast volumes of sediment by the Yangtze River and the related evolution of sedimentary systems in East Asia [13–17]. Although many methods have been used to study the provenance of the sediments of the Yangtze, the origin and evolution of the Yangtze River Basin remain debated [18]. Some previous studies have argued that sediment derived from the upper Yangtze River Basin first appeared in the middle–lower Yangtze River Basin during the Pleistocene [19–21], whereas other studies have proposed that the Yangtze River developed into a large river similar to the modern Yangtze, probably during the Oligocene and no later than the end of the Neogene [10,22–24]. It is generally accepted that there have been two key capture points during the evolution of the Yangtze: the First Bend in the Shigu area and the Three Gorges valley [22]. In particular, the Three Gorges area, which is the link between the upper and the middle–lower Yangtze, has become a major focus of research.

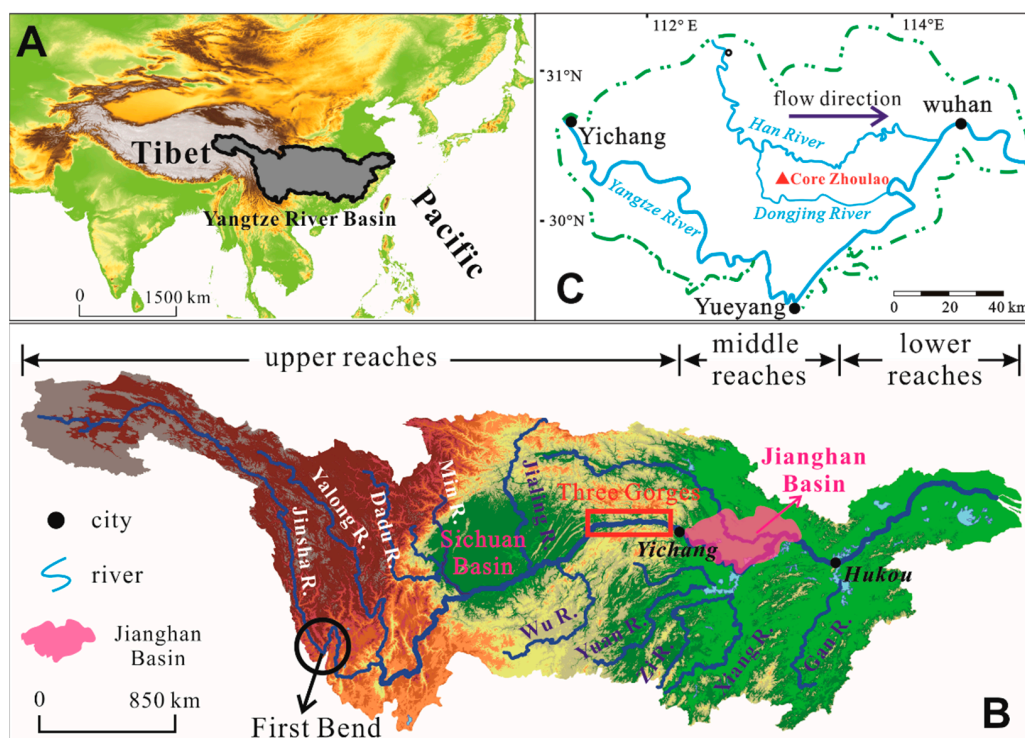


Figure 1. Sketch map showing the locations of the Yangtze River Basin (A), Jiangnan Basin (B), and the Zhoulao borehole (C). (A) The Yangtze River originates from the Tibetan Plateau and discharges into the Pacific; (B) locations of the two key capture points during the evolution of the Yangtze: the First Bend (black circle) and the Three Gorges (red rectangle). Additionally shown are the locations of the Sichuan and Jiangnan basins located to the west and just downstream of the Three Gorges, respectively; (C) location of the Zhoulao borehole in the depo-center of the Jiangnan Basin.

The Jiangnan Basin, located just below the outlet of the Three Gorges [25] (Figure 1b), is the closest and most sensitive depocenter related to the incision of the Three Gorges. Detrital zircon U–Pb dating has suggested that material eroded from the Tibetan Plateau reached the Jiangnan Basin at ca. 0.8 Ma, which implies that the Three Gorges valley was incised at the same time [26]. However, rare earth elements (REE) and Nd isotopic data indicate that the modern Yangtze River was established no later than the beginning of the Quaternary (2.58 Ma) [9], whereas detrital K-feldspar Pb isotope compositions show that feldspars from the Songpan-Ganzi terrane were already being delivered to the Jiangnan Basin by 3.4 Ma. Although these studies have provided important constraints on sediment provenance, at present there is no consensus regarding the timing of formation of the Three Gorges.

Numerous previous studies have established that fluvial sediments, especially assemblages of heavy minerals, record the source or provenance terrain and geology from which they were derived, thus providing insights into sedimentary transport systems [27–30]. Heavy mineral analysis has been shown to be a sensitive and robust technique for constraining sediment provenance and has been successfully applied in interpreting the provenance of modern Yangtze River sediments [30]. Heavy minerals are reliable and robust indicators of sedimentary sources because of their durability and stability during parent rock mechanical disaggregation and subsequent sediment abrasion, sorting, erosion, weathering, delivery, and deposition. However, this technique has not been applied to tracing the provenance of ancient fluvial sediments of the Yangtze River Basin.

In this study, we analyze variations in the heavy mineral assemblage of Pliocene–Pleistocene sediments in the Jiangnan Basin, middle Yangtze River Basin, to provide information regarding the timing of incision of the Three Gorges. The aims of the present contribution were to: (1) establish the temporal variation in heavy mineral assemblages of late Cenozoic sediments in the Jiangnan Basin; (2) determine the factors controlling the composition of these heavy mineral assemblages; (3) constrain the evolution of the provenance of late Cenozoic sediments in the Jiangnan Basin and identify the implications for the channelization/incision of the Three Gorges valley.

2. The Yangtze River Basin

2.1. River Setting

The Yangtze River is the largest river in Asia and the third-largest river in the world, with a length of >6300 km and a catchment area of $\sim 1.8 \times 10^6$ km² [31]. It is located between 24°27′–35°44′ N and 90°33′–122°19′ E. Traditionally, the Yangtze River has been divided into the upper, middle, and lower reaches [32] (Figure 1b). The Yangtze River drainage basin consists of complex strata ranging in age from Archean to Quaternary [33]. The Emeishan Large Igneous Province is the main mafic source rock in the upper Yangtze [34]. Loose Quaternary sediments and Paleozoic sedimentary rocks are extensively exposed in the middle–lower reaches of the Yangtze River [35] (Figure 2).

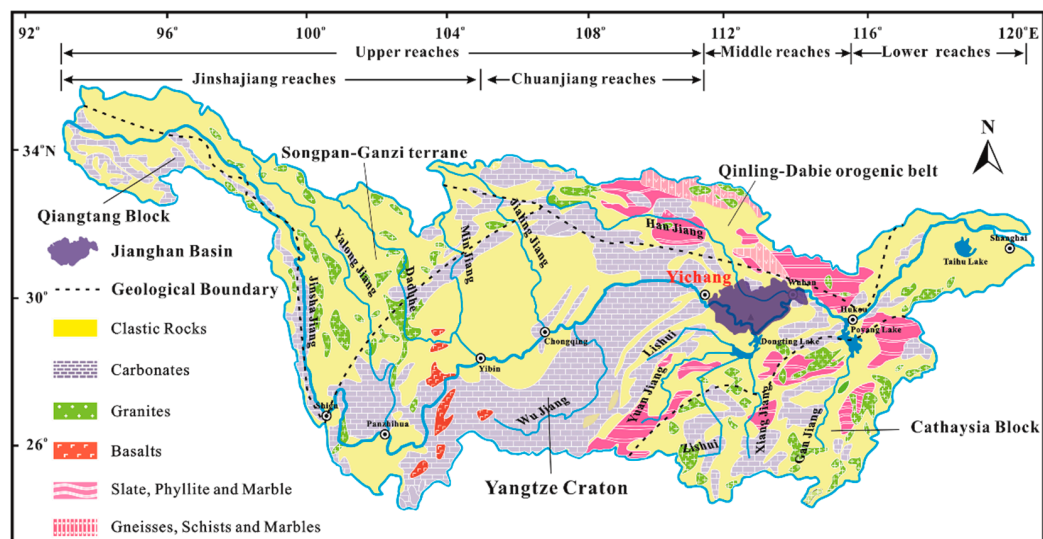


Figure 2. Geological map of the Yangtze River Basin (modified after Shao et al., 2012 [9]).

2.2. The Jiangnan Basin

The Jiangnan Basin is a Mesozoic—Cenozoic basin located just downstream of the Three Gorges. It is situated in the area of the middle Yangtze River and lower Hanjiang River between 29°26′–30°23′ N and 111°30′–114°32′ E (Figures 1B and 2) [36]. The Yangtze River crosses the entire Jiangnan Basin from west to east. The Jiangnan Basin is a depression belt of the Neo-Cathaysian structural system, with its landforms having originated from the Late Jurassic, controlled by the E–W-trending Qinling and Nanling structural belts [37]. Since the early Tertiary, the Jiangnan Basin has been in a state of subsidence, although Quaternary subsidence has been dominant and is concentrated in the Xinhe area. The lithofacies are fluvial–lacustrine facies showing a typical interlayered structure. The Jiangnan Basin is an important catchment basin in which voluminous sedimentary materials have been deposited by the upper Yangtze River. With the continuous accumulation of deposits sustained over a long time, especially during the late Cenozoic, the Jiangnan Basin provides an ideal material record for reconstructing the evolution of the Yangtze River [38].

2.3. The Late Cenozoic Zhoulao Drillcore

A continuous core was obtained from the Zhoulao drillhole in the Qianjiang Depression, Jiangnan Basin (Figure 1c). The Zhoulao core provides the best available magnetic stratigraphic column of the Jiangnan Basin. The magnetic stratigraphic framework of the core has been reported by Zhang et al. [21] (Figure 3) and shows a record of the Brunhes—Matuyama boundary (ca. 0.78 Ma) at 81 m depth and the Matuyama—Gauss boundary (ca. 2.58 Ma) at 250 m. The late Cenozoic (since 3.0 Ma) sedimentation record in the central Jiangnan Basin appears to be continuous. The final drilling depth of the Zhoulao drillhole was 300.49 m, with an average recovery rate of 85%. The average deposition rate of the Zhoulao core is 100 m/Ma.

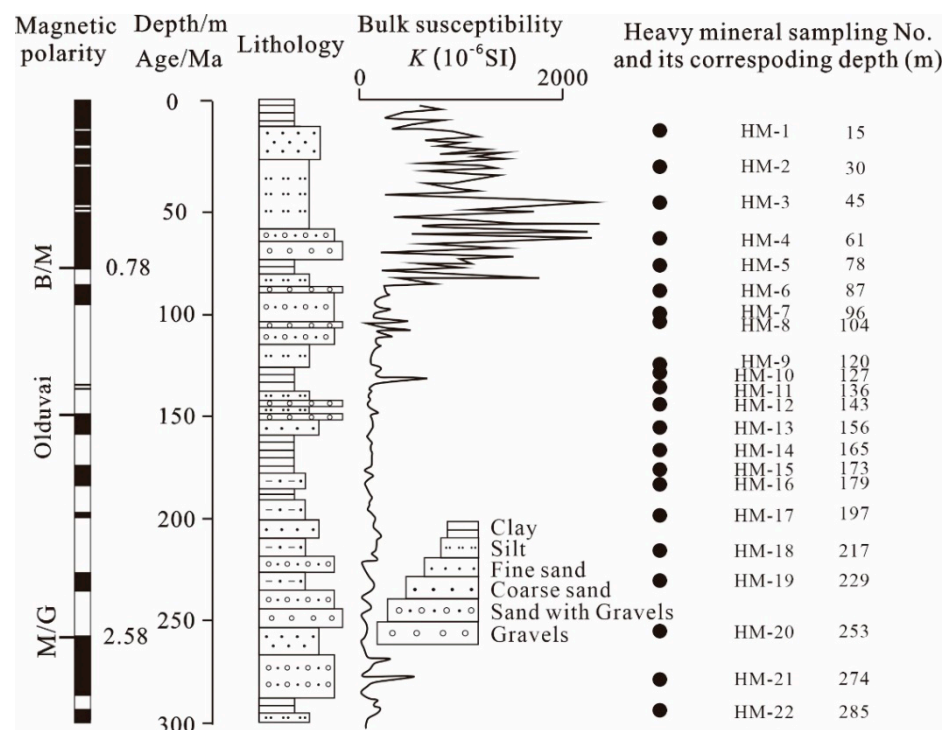


Figure 3. Magnetic polarity and lithology of late Cenozoic sediments in the Jiangnan Basin (Zhoulao core), as well as heavy mineral sampling numbers and corresponding depths. HM: heavy mineral; B/M: Brunhes—Matuyama boundary; M/G: Matuyama—Gauss boundary; the black dot represents sampling site.

3. Sampling and Method

A total of 22 samples were collected from the Zhoulao core. Sampling information, including sample numbers and corresponding depths, is presented in Table 1 and Figure 3. The experimental procedure was as follows. First, a 1 kg sample was taken from each sample after drying, immersed in clear water for 48 h, then sieved to obtain the 0.125–0.063 mm fraction, which was weighed using an electronic balance. Second, a 10 g sample was taken by separating the heavy and light minerals using bromoform (density of 2.89 g/cm³). After drying at a temperature of 60 °C, the total content of heavy minerals was obtained by weighing. Third, 10 view fields were selected using the strip method under a microscope to identify heavy minerals, with the mean value of these determinations being used to reduce errors. Several samples were ground into thin-sections to allow confirmation of heavy mineral identification under a polarizing microscope. The number of grains analyzed was more than 600 for every heavy mineral sample, on which basis the percentage of each type of heavy mineral was determined [39–42]. Because the samples are of the same size fraction, these percentage values represent volume percentages. Finally, the weight of each heavy mineral was calculated using the volume percentage and density.

Table 1. Heavy mineral contents of the Zhoulao core.

| Sample Number | Sampling Depth (m) | Total Weight of Sample (g) | Total Weight of Heavy Minerals (g) | % Content of Heavy Minerals | Zircon | Apatite | Tourmaline | Titanite | Kyanite | Epidote | Hornblende | Tremolite | Pyroxene | Garnet | Leucosene | Rutile | Glauconite | Chlorite | Anatase | Pyrite | Hematite-Limonite | Ilmenite | Magnetite | Allanite | Debris Affected by Iron |
|---------------|--------------------|----------------------------|------------------------------------|-----------------------------|--------|---------|------------|----------|---------|---------|------------|-----------|----------|--------|-----------|--------|------------|----------|---------|--------|-------------------|----------|-----------|----------|-------------------------|
| 1 | 15 | 550 | 7.40 | 1.35 | 3.08 | 0.38 | 3.30 | 3.64 | 0.13 | 13.40 | 9.22 | 0.11 | 7.23 | 8.30 | 1.42 | 0.81 | 0.51 | 16.36 | 1.39 | 0.00 | 23.82 | 19.57 | 12.04 | 0.68 | 9.25 |
| 2 | 30 | 520 | 9.10 | 1.75 | 4.04 | 1.65 | 1.44 | 4.77 | 0.50 | 19.15 | 16.61 | 1.44 | 9.48 | 16.31 | 1.86 | 4.23 | 0.94 | 19.80 | 3.63 | 0.00 | 25.37 | 19.24 | 13.52 | 1.79 | 9.43 |
| 3 | 45 | 150 | 2.83 | 1.89 | 0.65 | 3.53 | 0.15 | 3.40 | 0.18 | 20.48 | 20.99 | 0.15 | 11.83 | 25.19 | 1.99 | 0.45 | 0.00 | 19.40 | 0.19 | few | 12.52 | 36.57 | 19.28 | 0.19 | 11.53 |
| 4 | 61 | 340 | 3.02 | 0.89 | 1.91 | 0.78 | 0.14 | 0.23 | 0.08 | 6.04 | 3.57 | 0.00 | 2.24 | 6.00 | 2.64 | 0.10 | 0.64 | 7.80 | 0.09 | 0.14 | 8.30 | 24.25 | 18.11 | 0.08 | 5.73 |
| 5 | 78 | 240 | 6.20 | 2.58 | 2.94 | 2.40 | 0.21 | 6.94 | 0.24 | 32.50 | 24.16 | 1.05 | 2.30 | 23.72 | 10.81 | 0.31 | 0.00 | 19.20 | 0.26 | 0.42 | 53.94 | 12.44 | 42.62 | 2.60 | 19.60 |
| 6 | 87 | 340 | 7.30 | 2.15 | 7.29 | 1.98 | 0.52 | 3.82 | 1.00 | 26.85 | 9.07 | 0.52 | 9.49 | 21.77 | 2.23 | 0.76 | 0.49 | 17.84 | 2.18 | few | 42.21 | 28.25 | 21.66 | 0.64 | 16.19 |
| 7 | 96 | 190 | 3.72 | 1.96 | 2.36 | 1.93 | 1.68 | 1.86 | few | 48.45 | 19.39 | few | 12.91 | 12.69 | 4.34 | 1.97 | 1.57 | 30.81 | 0.21 | 0.34 | 6.83 | 27.45 | 5.26 | 0.00 | 15.73 |
| 8 | 104 | 80 | 3.45 | 4.31 | 5.04 | 4.11 | 0.36 | 1.98 | few | 87.59 | 22.60 | 0.72 | 23.64 | 67.80 | 4.64 | 2.64 | 6.72 | 69.95 | 0.45 | 0.72 | 9.74 | 95.97 | 5.62 | 0.89 | 20.17 |
| 9 | 120 | 620 | 2.60 | 0.42 | 2.07 | 1.27 | 0.37 | 2.44 | few | 6.13 | 1.55 | 0.00 | 2.02 | 2.32 | 2.86 | 0.54 | 0.14 | 4.65 | 0.93 | 0.15 | 5.50 | 4.93 | 0.58 | 0.46 | 3.11 |
| 10 | 127 | 410 | 2.80 | 0.68 | 3.46 | 1.41 | 0.25 | 2.04 | 0.07 | 13.64 | 3.23 | 0.06 | 3.38 | 2.32 | 3.18 | 0.90 | 0.58 | 10.58 | 0.47 | 0.50 | 10.01 | 6.39 | 0.96 | 0.31 | 4.61 |
| 11 | 136 | 700 | 3.90 | 0.56 | 4.60 | 0.27 | 0.23 | 2.58 | 0.05 | 4.67 | 2.94 | few | 2.05 | 2.94 | 2.41 | 0.69 | 0.13 | 6.96 | 1.18 | few | 2.54 | 18.05 | 0.15 | 0.23 | 3.06 |
| 12 | 143 | 300 | 3.30 | 1.10 | 7.56 | 0.41 | 0.45 | 3.97 | few | 14.93 | 8.47 | few | 3.94 | 7.91 | 3.48 | 3.95 | 0.50 | 12.34 | 2.27 | few | 7.30 | 23.99 | 1.40 | 0.45 | 6.72 |
| 13 | 156 | 410 | 8.51 | 2.08 | 12.03 | 1.23 | 0.64 | 0.47 | 0.50 | 33.25 | 13.48 | 0.21 | 7.05 | 18.88 | 8.30 | 1.57 | 1.00 | 27.00 | 0.54 | 4.32 | 2.90 | 54.07 | 3.35 | 0.80 | 16.04 |
| 14 | 165 | 400 | 2.13 | 0.53 | 0.64 | 0.26 | 0.46 | 0.50 | few | 10.60 | 4.30 | 0.05 | 3.50 | 2.87 | 2.35 | 0.67 | 0.85 | 10.96 | 0.06 | 0.09 | 0.62 | 10.14 | 0.07 | few | 4.26 |
| 15 | 173 | 500 | 3.00 | 0.60 | 2.83 | 1.73 | 0.50 | 1.11 | 0.06 | 10.05 | 2.11 | few | 3.31 | 4.44 | 3.90 | 0.59 | 0.38 | 5.19 | 1.91 | 0.30 | 7.51 | 8.97 | 0.79 | 0.63 | 3.77 |
| 16 | 179 | 70 | 0.60 | 0.86 | 2.00 | 0.25 | 1.43 | 0.08 | 0.08 | 10.28 | 6.74 | 0.07 | 6.26 | 4.49 | 2.76 | 0.21 | 0.67 | 13.90 | 0.09 | 7.20 | 7.74 | 8.47 | 2.23 | 0.09 | 10.68 |
| 17 | 197 | 750 | 1.90 | 0.25 | 1.27 | 1.30 | 0.23 | 0.75 | 0.00 | 5.77 | 0.24 | 0.00 | 0.75 | 1.71 | 2.05 | 0.20 | 0.11 | 1.56 | 0.57 | 0.18 | 2.76 | 3.02 | 1.06 | 0.14 | 1.69 |
| 18 | 217 | 300 | 5.30 | 1.77 | 4.02 | 1.15 | 1.43 | 3.17 | few | 41.29 | 9.01 | few | 3.14 | 10.82 | 7.40 | 2.10 | 2.68 | 18.05 | 3.62 | 5.78 | 9.71 | 42.53 | 2.24 | 0.53 | 8.04 |
| 19 | 229 | 260 | 2.90 | 1.12 | 7.75 | 2.11 | 0.92 | 2.03 | 0.21 | 22.44 | 4.82 | few | 3.03 | 5.79 | 7.13 | 0.68 | 0.17 | 9.49 | 1.16 | 1.86 | 16.21 | 13.66 | 2.88 | 0.69 | 8.61 |
| 20 | 253 | 170 | 2.20 | 1.29 | 4.53 | 0.62 | 0.54 | 4.75 | few | 22.63 | 6.76 | few | 2.36 | 6.76 | 8.32 | 0.79 | 1.01 | 22.20 | 2.71 | 0.22 | 4.37 | 30.31 | 0.17 | 0.40 | 10.06 |
| 21 | 274 | 290 | 2.40 | 0.83 | 8.32 | 0.53 | 0.66 | 3.64 | few | 10.94 | 1.38 | few | 0.72 | 4.97 | 5.10 | 0.97 | 0.12 | 10.56 | 2.49 | 1.06 | 2.68 | 23.45 | 0.10 | 0.16 | 4.93 |
| 22 | 285 | 310 | 2.01 | 0.65 | 2.20 | 0.60 | 0.52 | 0.58 | 0.06 | 11.00 | 1.64 | 0.10 | 1.72 | 7.23 | 2.70 | 0.77 | 0.49 | 8.97 | 0.33 | 3.16 | 1.42 | 14.73 | 1.63 | 0.13 | 4.89 |

4. Analysis and Results

4.1. Heavy Mineral Species and Heavy Mineral Concentration Index

Statistical results of heavy minerals for the 22 analyzed samples are presented in Table 1. Twenty-one different heavy minerals were detected in the Zhoulao core sediment samples. Several minerals with densities of $>2.89 \text{ g/cm}^3$ account for 83.54% of the total heavy mineral content, including magnetite, amphibole, pyroxene, epidote, chlorite, garnet, ilmenite, hematite–limonite, and iron-stained detritus, whereas zircon, apatite, titanite, leucoxene, anatase, and pyrite account for 13.61%, and the other 11 heavy minerals account for 2.85%.

The heavy mineral concentration (HMC) index measures the abundance of heavy minerals contained in fluvial sediments [29]. The HMC index measures the production of heavy mineral grains by source rock and is calculated as the heavy mineral content of a sample expressed as a percentage. Figure 4 shows that contents of the main minerals vary substantially with depth. A marked change is observed in heavy mineral contents at sample 8 (104 m depth, gray band in Figure 4).

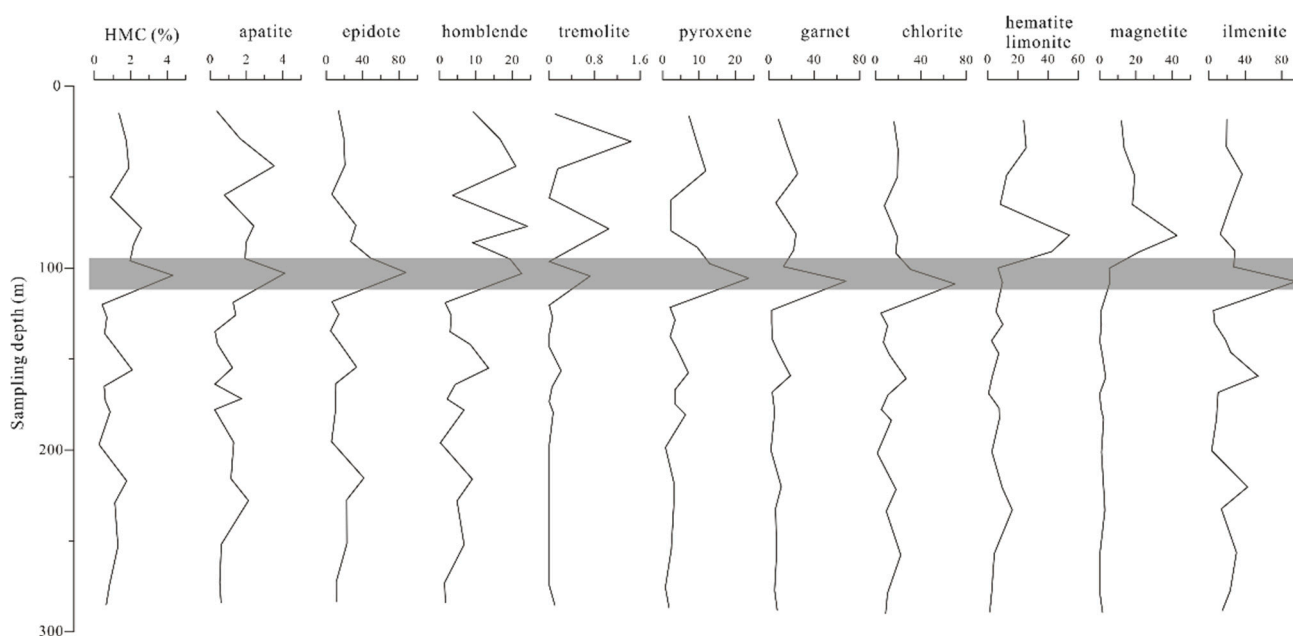


Figure 4. Variation in main heavy mineral contents of the Zhoulao core with depth. The gray rectangle marks where heavy mineral contents show an obvious change at a depth of ~110 m.

The mean value of HMC for the whole core is 1.35%, but the maximum (4.31%) appears in sample 8. The mean HMC value of samples 1–8 is 2.11%, whereas that of samples 9–22 is 0.91%. Taking the overall mean of 1.35% as the background value, the mean value of samples 1–8 is 0.76% higher than the background value, whereas that of samples 9–22 is 0.44% lower. Therefore, we divided the core into two sections, corresponding to samples 1–8 and samples 9–22, respectively.

4.2. Heavy Mineral Assemblages

In addition to the variation in HMC, we also made a comparison of the heavy mineral assemblages between the two sections. Figure 5 shows that samples 22–9 are characterized as a heavy mineral assemblage of zircon, apatite, epidote, leucoxene, rutile, chlorite, ilmenite, anatase, pyrite, and titanite (white rectangle in group 1), whereas samples 8–1 are characterized by hornblende, pyroxene, garnet, hematite–limonite, and magnetite (black rectangle in group 2). These results also show that the sediment source area underwent a marked change at the time, corresponding to a depth of 104 m in the Zhoulao core.

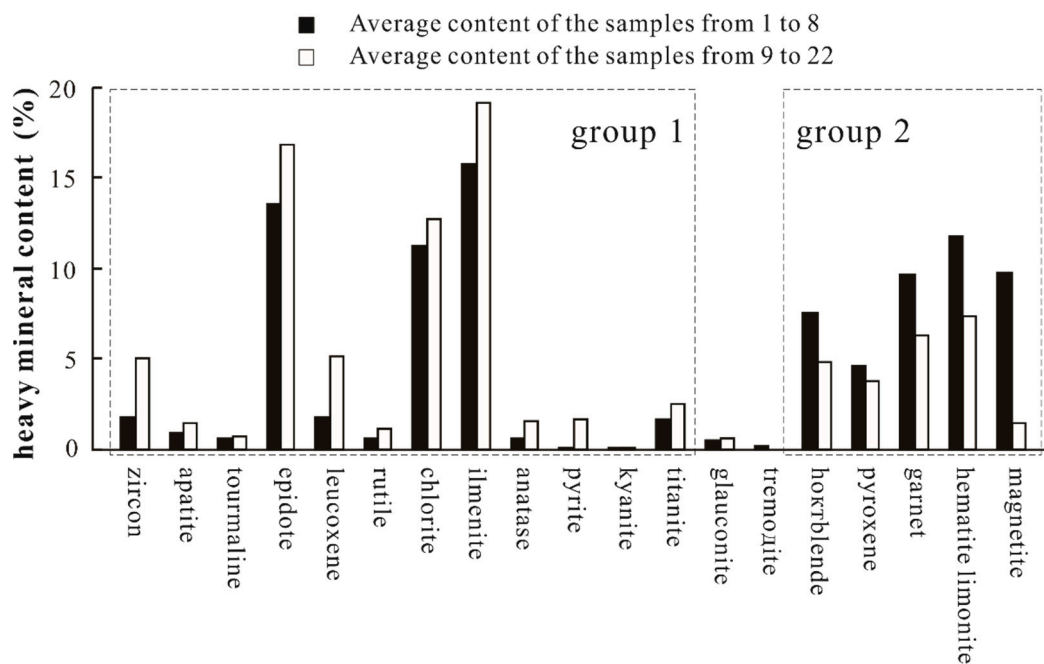


Figure 5. Comparison of heavy mineral assemblages between samples 22 to 9 and samples 8 to 1. In group 1, the average content of each heavy mineral of samples 8 to 1 is less than that of samples 22 to 9; in group 2, the average content of each heavy mineral of samples 8 to 1 is more than that of samples 22 to 9.

4.3. Apatite–Tourmaline, Garnet–Zircon, and Zircon–Tourmaline–Rutile Index Analysis

Morton and Hallsworth [31] proposed that the main controls on heavy mineral assemblages in fluvial sediments are (1) hydraulics, which fractionates the relative abundance of minerals with different hydraulic behavior; (2) burial diagenesis, which reduces mineral diversity through progressive dissolution of unstable mineral species. Morton and Hallsworth [31] proposed the ATi (apatite-tourmaline), GZi (garnet-zircon), and ZTR (zircon-tourmaline-rutile) indexes to understand the transportation processes of sediments. These three indexes are defined as:

$$\text{ATi} = 100 \times \text{apatite\%} / (\text{apatite\%} + \text{tourmaline\%}) \quad (1)$$

$$\text{GZi} = 100 \times \text{garnet\%} / (\text{garnet\%} + \text{zircon\%}) \quad (2)$$

$$\text{ZTR} = \text{zircon\%} + \text{tourmaline\%} + \text{rutile\%} \quad (3)$$

ATi can be used to measure the extent of weathering during alluvial storage. In fluvial sediments deposited in humid tropical settings, the ratio of apatite to tourmaline decreases substantially over time during alluvial storage, whereas the effect on other indexes is less, meaning that variations in ATi can at least partially reflect the degree of weathering during alluvial storage. ATi can also be used to indicate changes in provenance combined with GZi and ZTR.

Table 2 and Figure 6 show that there is a significant difference in each of ATi, GZi, and ZTR between samples 22–9 and samples 8–1. The values of ATi and GZi increase, whereas the value of ZTR decreases from 120 to 100 m depth in the Zhoulao core. The increase in ATi may be due to two reasons: the first is that the source rock changed from one with a lower abundance of apatite to one with a higher abundance during the time corresponding to this depth interval; the second is that the depositional environment changed to one characterized by stronger hydrodynamics and a higher deposition rate, which caused the weathering of apatite to weaken. The increase in GZi was caused by an increase in the proportion of source composed of metamorphic rock, which caused garnet content in the core sediments to increase. The decrease in ZTR indicates that the mineralogical

maturity reduced owing to increasing rates of weathering, denudation, and deposition. Thus, all three curves in Figure 6 show that the depositional environment changed at the time corresponding to 110 m in the Zhoulao core to one characterized by strengthened hydrodynamics and increased sediment volume, suggesting that the drainage system also had to make a corresponding adjustment.

Table 2. Variation in ATi, GZi, and ZTR indexes through the Zhoulao core.

| Sample No. | ATi | GZi | ZTR | Sample No. | ATi | GZi | ZTR |
|------------|-----|-----|-----|------------|-----|-----|------|
| 1 | 9 | 75 | 5.5 | 12 | 44 | 54 | 9.5 |
| 2 | 50 | 82 | 5.0 | 13 | 63 | 64 | 4.8 |
| 3 | 95 | 98 | 0.6 | 14 | 33 | 83 | 3.0 |
| 4 | 83 | 78 | 2.3 | 15 | 75 | 64 | 5.8 |
| 5 | 91 | 90 | 1.2 | 16 | 13 | 71 | 4.2 |
| 6 | 77 | 77 | 3.6 | 17 | 83 | 60 | 5.6 |
| 7 | 50 | 86 | 2.8 | 18 | 41 | 75 | 4.0 |
| 8 | 91 | 94 | 1.6 | 19 | 67 | 45 | 7.5 |
| 9 | 75 | 56 | 6.0 | 20 | 50 | 63 | 4.0 |
| 10 | 83 | 43 | 5.4 | 21 | 41 | 40 | 11.0 |
| 11 | 50 | 42 | 8.5 | 22 | 50 | 79 | 5.0 |

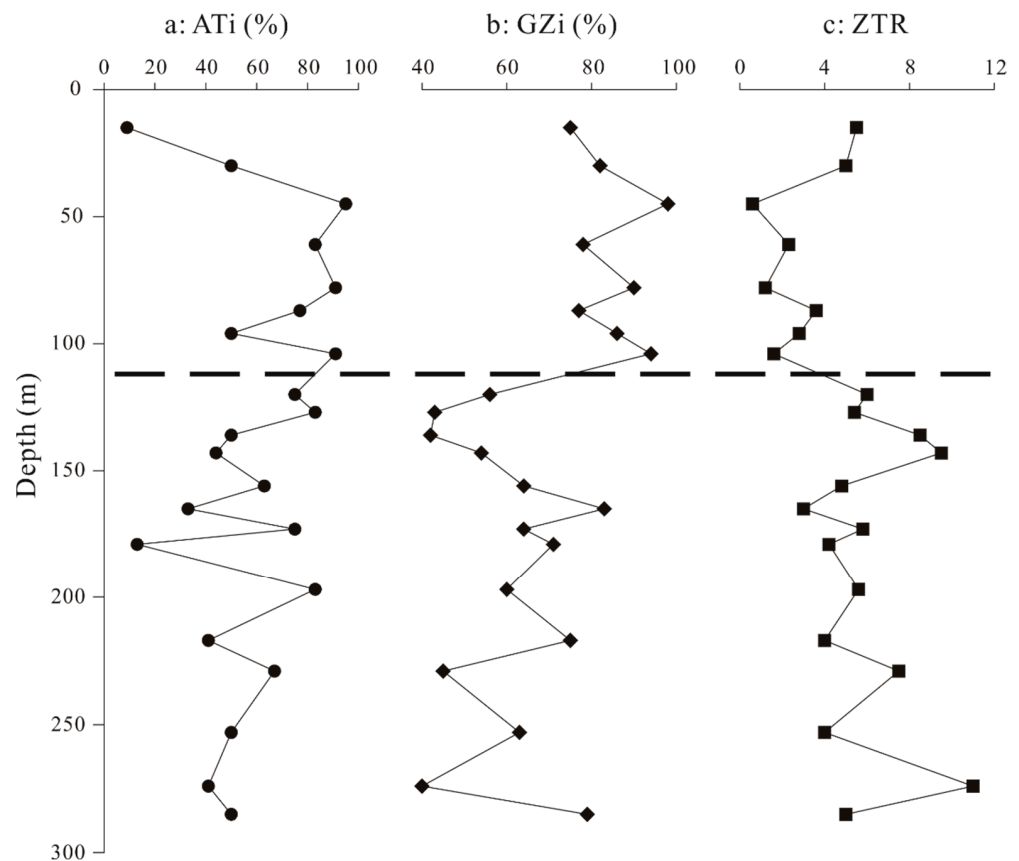


Figure 6. Variations in the indexes of ATi, GZi, and ZTR for the Zhoulao core sediments. All three curves show a significant transition at a depth of about 110 m.

5. Discussion

5.1. Provenance of Diagnostic Heavy Minerals

Figures 4–6 show that there is a marked difference in heavy mineral assemblage between the lower section of the Zhoulao core (samples 22–9) and the upper section (samples 8–1), suggesting that the source of the sediments underwent a pronounced change. It is worth noting that the heavy mineral assemblage of the upper section is similar to that of modern surface fluvial sediments and low-terrace fluvial sediments of the Yangtze River, which are characterized by magnetite, hornblende, pyroxene, garnet, epidote, limonite, and ilmenite [20,30]. Enriched epidote, garnet, and chlorite in the upper section are typical minerals sourced from metamorphic rocks and secondary minerals of ferromagnesian minerals, such as hornblende, pyroxene, and biotite [20,30]. In addition, ilmenite, magnetite, pyroxene, and hornblende are sourced from mafic–ultramafic volcanic rock, whereas hematite and limonite are supplied mainly by metasedimentary rock [35]. This suggests that areas of metamorphic and mafic–ultramafic volcanic rock in the upper Yangtze River Basin are the main sedimentary source areas. Diagnostic zircon, leucoxene, epidote, and chlorite are sourced mainly from sedimentary rock, which crops out mainly in the middle–lower Yangtze River Basin, especially the Jiangnan Basin [37] (Figure 2).

Before incision of the Three Gorges valley, the sediments of the Jiangnan Basin were supplied by adjacent areas and the Han River catchment, which are located on sedimentary rock [30]. This sourcing of sediment from local areas and the Han catchment is consistent with the heavy mineral assemblage of the lower section of the Zhoulao core. The upper Yangtze River Basin, west of the Three Gorges, consists mainly of mafic–ultramafic volcanic rock and metamorphic rock, especially within the Jialing River catchment. In addition, Emeishan basalt and vanadium titanite in the Panzhihua area have made a contribution of magnetite to the upper section of the Zhoulao core and also to modern surface Yangtze sediments and low-terrace fluvial sediments [30]. After incision of the Three Gorges, materials from the upper Yangtze River Basin were able to be transported to the middle–lower reaches and were deposited mainly in the Jiangnan Basin, just downstream of the Three Gorges.

5.2. Comparison of Heavy Metals with Other Provenance Indicators for the Zhoulao Core

In previous studies, numerous provenance indicators have been applied to trace the sediment provenance of the Zhoulao core to constrain the formation of the Three Gorges. Magnetic parameter analysis of the Zhoulao core [21] has shown that the contents of coarse materials and stable magnetic minerals both increase markedly above a depth of ~110 m (Figure 3). In addition, the magnetic susceptibility of the sediments, their saturation isothermal remanent magnetization, and the magnetic susceptibility values of anhysteretic remanent magnetism also increase sharply at the same depth, indicating an important adjustment event in the hydrological–sedimentary environment of the Jiangnan Plain related to incision of the Three Gorges valley. Taking into consideration the paleomagnetic framework, Zhang et al. [21] proposed that the timing of channelization of the Three Gorges valley probably occurred between 1.17 and 1.12 Ma. Pyroxene contents of the Zhoulao core change abruptly at ~104 m [32], and provenance indicator trace-element contents and ratios [33] (ΣREE , Y, Th, U, Th/Sc, Co/Th, La/Sc, and Cr/Cu) become lower above ~125 m depth, which has been interpreted as evidence that the Three Gorges was incised at 1.25 Ma (Figure 7). All of these previous studies constrained the timing of formation of the Three Gorges during the Early Pleistocene.

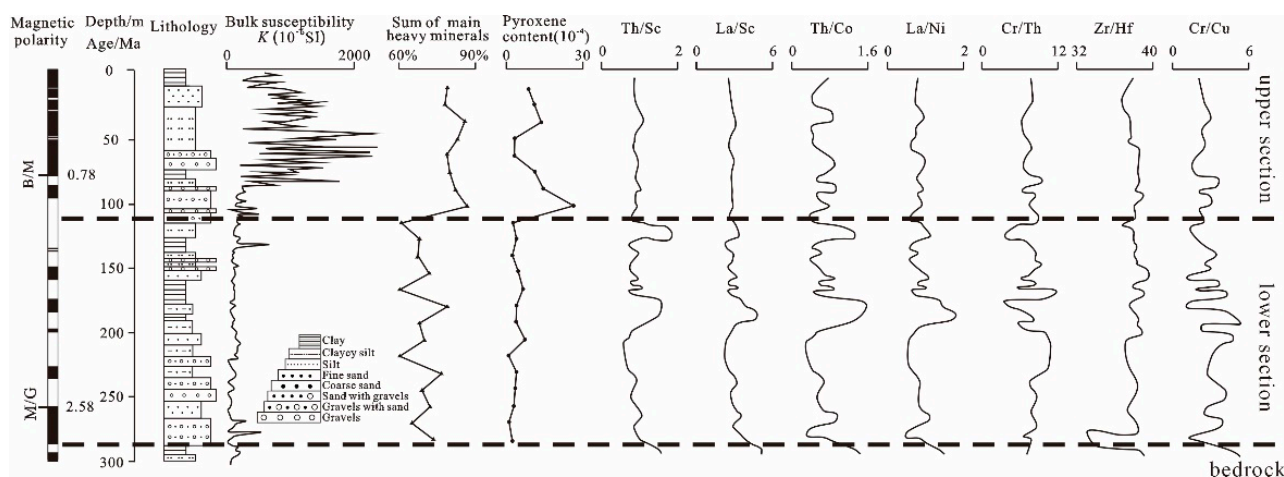


Figure 7. Variation in provenance indicator values of the Zhoulao core. Lithology, magnetic characteristics, heavy mineral assemblage, pyroxene content, and trace-element patterns suggest that the sediment provenance underwent a major change at a depth of ~110 m in the Zhoulao core.

5.3. Implications for the Timing of Incision of the Three Gorges

Our provenance interpretation shows that sediments of the lower section (below 110 m) of the Zhoulao core were sourced from the area surrounding the Jiangnan Basin, whereas materials of the upper section (above 110 m) were supplied mainly by the upper Yangtze River Basin, west of the Three Gorges. This transition in provenance of sediment in the Jiangnan Basin reflects the incision of the Three Gorges. Combining our provenance information with paleomagnetic polarity chronology [21], we propose that the Three Gorges valley was incised at about 1.1 Ma, which allowed throughflow of water and sediment into the Jiangnan Basin.

6. Conclusions

The Jiangnan Basin is located just downstream of the Three Gorges valley and is a crucial location for understanding the evolution of this valley. Our study of the provenance of sedimentary deposits in the Jiangnan Basin has shed light on the geological origin of the sediments, the morphological evolution of the Three Gorges valley, and the development of the Yangtze River valley. In this study, we obtained 22 samples from late Cenozoic sediments obtained from the Zhoulao core in the central Jiangnan Basin for heavy mineral assemblage analysis to trace their provenance.

Results of the study show that there is a marked difference in the heavy mineral assemblage between the lower (below 110 m) and upper (above 110 m) sections of the Zhoulao core. The lower section has a heavy mineral assemblage of zircon, epidote, leucoxene, rutile, anatase, pyrite, and titanite, whereas the upper section has an assemblage of hornblende, pyroxene, garnet, hematite–limonite, and magnetite. The sediments in the lower section were sourced from the area surrounding the Jiangnan Basin, but those of the upper section were supplied mainly by the upper Yangtze River Basin. This sediment provenance transition marks the incision of the Three Gorges, which allowed sediment to be transported into the Jiangnan Basin and deposited there. Combining our provenance information with paleomagnetic polarity chronology, we propose that the Three Gorges were incised at about 1.1 Ma. Our results are consistent with patterns of other provenance indicators, including magnetic parameter analysis, lithology, pyroxene content, and trace-element characteristics.

Author Contributions: C.K. and C.L. formulated the topic of the study and performed the project; C.K., C.W., Y.Z. and H.J. performed fieldwork and sample collection; C.K., Y.L. and R.G. analyzed the data and wrote the manuscript. All authors have read and agreed to the published version of the manuscript.

Funding: This work was supported by grants from the National Natural Science Foundation of China (No. 41877292 and No. 42002203).

Data Availability Statement: All data of the study can be found in Tables 1 and 2.

Conflicts of Interest: The authors declare no conflict of interest.

References

1. Chen, Z.; Li, J.; Shen, H.; Zhanghua, W. Yangtze River of China: Historical analysis of discharge variability and sediment flux. *Geomorphology* **2001**, *41*, 77–91. [[CrossRef](#)]
2. Wu, W. Sediment geochemistry of large rivers originating from the Tibetan Plateau: Provenance and weathering. *Quat. Int.* **2012**, *279–280*, 542. [[CrossRef](#)]
3. Wang, K.; Zheng, H.; Tada, R.; Irino, T.; Zheng, Y.; Saito, K.; Karasuda, A. Millennial-scale East Asian Summer Monsoon variability recorded in grain size and provenance of mud belt sediments on the inner shelf of the East China Sea during mid-to late Holocene. *Quat. Int.* **2014**, *349*, 79–89. [[CrossRef](#)]
4. Xu, J.; Yang, D.; Yi, Y.; Lei, Z.; Chen, J.; Yang, W. Spatial and temporal variation of runoff in the Yangtze River basin during the past 40 years. *Quat. Int.* **2008**, *186*, 32–42. [[CrossRef](#)]
5. Wei, C.; Liu, C.; Li, W.; Zhang, Z.; Zhang, H.; Zhao, J.; Zhang, L. Nature ESR signals of quartz E'center shed new light on river sediments provenance: A case study in southeast margin of the Tibet Plateau. *Quat. Int.* **2017**, *454*, 38–44. [[CrossRef](#)]
6. Liu, S.; Mi, B.; Fang, X.; Li, X.; Pan, H.-J.; Chen, M.-T.; Shi, X. A preliminary study of a sediment core drilled from the mud area on the inner shelf of the East China Sea: Implications for paleoclimatic changes during the fast transgression period (13 ka BP–8 ka BP). *Quat. Int.* **2017**, *441*, 35–50. [[CrossRef](#)]
7. Li, C.; Yang, S.; Lian, E.; Wang, Q.; Fan, D.; Huang, X. Chemical speciation of iron in sediments from the Changjiang Estuary and East China Sea: Iron cycle and paleoenvironmental implications. *Quat. Int.* **2017**, *452*, 116–128. [[CrossRef](#)]
8. Clift, P.D.; Blusztajn, J.; Nguyen, A.D. Large-scale drainage capture and surface uplift in eastern Tibet–SW China before 24 Ma inferred from sediments of the Hanoi Basin, Vietnam. *Geophys. Res. Lett.* **2006**, *33*, 33. [[CrossRef](#)]
9. Shao, L.; Yuan, S.; Kang, C.; Wang, J.; Li, T. Neodymium isotopic variations of the late Cenozoic sediments in the Jiangnan Basin: Implications for sediment source and evolution of the Yangtze River. *J. Asian Earth Sci.* **2012**, *45*, 57–64. [[CrossRef](#)]
10. Zheng, H.; Clift, P.D.; Wang, P.; Tada, R.; Jia, J.; He, M.; Jourdan, F. Pre-miocene birth of the Yangtze River. *Proc. Natl. Acad. Sci. USA* **2013**, *110*, 7556–7561. [[CrossRef](#)]
11. Lu, X.; Jiang, T. Larger Asian rivers: Shorter and longer term hydro-climate changes in humid and arid environments. *Quat. Int.* **2014**, *336*, 1–5. [[CrossRef](#)]
12. Zhang, Z.; Daly, J.S.; Li, C.A.; Tyrrell, S.; Sun, X.; Yan, Y.J. Sedimentary provenance constraints on drainage evolution models for SE Tibet: Evidence from detrital K-feldspar. *Geophys. Res. Lett.* **2017**, *44*, 4064–4073. [[CrossRef](#)]
13. Mao, L.; Mo, D.; Yang, J.; Guo, Y.; Lv, H. Rare earth elements geochemistry in surface floodplain sediments from the Xiangjiang River, middle reach of Changjiang River, China. *Quat. Int.* **2014**, *336*, 80–88. [[CrossRef](#)]
14. Bi, L.; Yang, S.; Zhao, Y.; Wang, Z.; Dou, Y.; Li, C.; Zheng, H. Provenance study of the Holocene sediments in the Changjiang (Yangtze River) estuary and inner shelf of the East China sea. *Quat. Int.* **2017**, *441*, 147–161. [[CrossRef](#)]
15. Hu, C.; Xu, Y.; Hu, C.; Wu, L.; Xu, G.; Yang, L. Genesis of the Qingyijiang River on the northern fringe of Mt. Huangshan, China, based on a combined analysis of gravel fabrics and ESR dates. *Quat. Int.* **2017**, *440*, 137–146. [[CrossRef](#)]
16. Pan, D.; Chen, T.; Zhan, Q.; Wang, Z. Mineral magnetic properties of Holocene sediments in the subaqueous Yangtze delta and the implications for human activity and early diagenesis. *Quat. Int.* **2017**, *459*, 133–143. [[CrossRef](#)]
17. Mi, B.; Liu, S.; Shi, X.; Li, X.; Pan, H.-J.; Chen, M.-T.; Wang, X. A high resolution record of rare earth element compositional changes from the mud deposit on the inner shelf of the East China Sea: Implications for paleoenvironmental changes. *Quat. Int.* **2017**, *447*, 35–45. [[CrossRef](#)]
18. Gu, J.; Chen, J.; Sun, Q.; Wang, Z.; Wei, Z.; Chen, Z. China's Yangtze delta: Geochemical fingerprints reflecting river connection to the sea. *Geomorphology* **2014**, *227*, 166–173. [[CrossRef](#)]
19. Li, J.; Xie, S.; Kuang, M. Geomorphic evolution of the Yangtze Gorges and the time of their formation. *Geomorphology* **2001**, *41*, 125–135. [[CrossRef](#)]
20. Xiang, F.; Zhu, L.; Wang, C.; Zhao, X.; Chen, H.; Yang, W. Quaternary sediment in the Yichang area: Implications for the formation of the Three Gorges of the Yangtze River. *Geomorphology* **2007**, *85*, 249–258. [[CrossRef](#)]
21. Zhang, Y.; Wang, Q.; Chen, L.; Ma, Y.; Kang, C. Magnetism parameters characteristics of drilling deposits in Jiangnan Plain and indication for forming of the Yangtze River Three Gorges. *Chin. Sci. Bull.* **2008**, *53*, 584–590. [[CrossRef](#)]
22. Clark, M.; Schoenbohm, L.; Royden, L.; Whipple, K.; Burchfiel, B.; Zhang, X.; Tang, W.; Wang, E.; Chen, L. Surface uplift, tectonics, and erosion of eastern Tibet from large-scale drainage patterns. *Tectonics* **2004**, *23*. [[CrossRef](#)]
23. Clift, P.D.; Long, H.V.; Hinton, R.; Ellam, R.M.; Hannigan, R.; Tan, M.T.; Blusztajn, J.; Duc, N.A. Geophysics, Geosystems, Evolving east Asian river systems reconstructed by trace element and Pb and Nd isotope variations in modern and ancient Red River-Song Hong sediments. *Geochem. Geophys. Geosystems* **2008**, *9*. [[CrossRef](#)]
24. Richardson, N.; Densmore, A.; Seward, D.; Wipf, M.; Yong, L. Did incision of the Three Gorges begin in the Eocene? *Geology* **2010**, *38*, 551–554. [[CrossRef](#)]

25. Li, F.; Zhu, C.; Wu, L.; Sun, W.; Liu, H.; Chyi, S.-J.; Kung, C.-L.; Zhu, G.; Wang, X. Environmental humidity changes inferred from multi-indicators in the Jiangnan Plain, Central China during the last 12,700 years. *Quat. Int.* **2014**, *349*, 68–78. [[CrossRef](#)]
26. Wang, J.; Yang, Y.; Shao, L.J. Detrital zircon geochronology and provenance of core sediments in Zhoukao Town, Jiangnan plain, China. *J. Earth Sci.-China* **2010**, *21*, 257–271. [[CrossRef](#)]
27. Garzanti, E.; Vezzoli, G.; Andò, S.; Paparella, P.; Clift, P.D.J.E.; Letters, P.S. Petrology of Indus River sands: A key to interpret erosion history of the Western Himalayan Syntaxis. *Earth Planet Sci. Lett.* **2005**, *229*, 287–302. [[CrossRef](#)]
28. Garzanti, E.; Andò, S.; Vezzoli, G.; Megid, A.A.A.; El Kammar, A.J.E.; Letters, P.S. Petrology of Nile River sands (Ethiopia and Sudan): Sediment budgets and erosion patterns. *Earth Planet Sci. Lett.* **2006**, *252*, 327–341. [[CrossRef](#)]
29. Garzanti, E.; Andò, S. Chapter 20 heavy mineral concentration in modern sands: Implications for provenance interpretation. *Dev. Sedimentol.* **2007**, *58*, 517–545.
30. Yang, S.; Wang, Z.; Guo, Y.; Li, C.; Cai, J. Heavy mineral compositions of the Changjiang (Yangtze River) sediments and their provenance-tracing implication. *J. Asian Earth Sci.* **2009**, *35*, 56–65. [[CrossRef](#)]
31. Zhang, Z.; Tyrrell, S.; Li, C.A.; Daly, J.S.; Sun, X.; Li, Q. Pb isotope compositions of detrital K-feldspar grains in the upper-middle Yangtze River system: Implications for sediment provenance and drainage evolution. *Geochem. Geophys. Geosystems.* **2014**, *15*, 2765–2779. [[CrossRef](#)]
32. Zheng, H.; Wei, X.; Tada, R.; Clift, P.D.; Wang, B.; Jourdan, F.; Wang, P.; He, M. Late Oligocene–early Miocene birth of the Taklimakan Desert. *Proc. Natl. Acad. Sci. USA* **2015**, *112*, 7662–7667. [[CrossRef](#)]
33. Saito, K.; Tada, R.; Zheng, H.; Irino, T.; Luo, C.; He, M.; Wang, K.; Suzuki, Y. ESR signal intensity of quartz in the fine-silt fraction of riverbed sediments from the Yangtze River: A provenance tracer for suspended particulate matter. *Prog. Earth Planet Sci.* **2017**, *4*, 4. [[CrossRef](#)]
34. Jiang, H.; Li, C.A.; Kang, C.; Zhang, Y.; Wei, C.; Zhao, J.; Li, Y. Provenance discrimination of upper Yangtze River basin sediments: New insights from heavy mineral signatures and detrital magnetite geochemistry. *Quat. Int.* **2020**, *568*, 79–89. [[CrossRef](#)]
35. Wei, C.; Voinchet, P.; Zhang, Y.; Bahain, J.-J.; Liu, C.; Kang, C.; Yin, G.; Sun, X.; Li, C. Chronology and provenance of the Yichang Gravel Layer deposits in the Jiangnan Basin, middle Yangtze River Valley, China: Implications for the timing of channelization of the Three Gorges Valley. *Quat. Int.* **2020**, *550*, 39–54. [[CrossRef](#)]
36. Zhang, Z.; Tyrrell, S.; Li, C.A.; Daly, J.S.; Sun, X.; Blowick, A.; Lin, X. Provenance of detrital K-feldspar in Jiangnan Basin sheds new light on the Pliocene–Pleistocene evolution of the Yangtze River. *Geol. Soc. Am. Bull.* **2016**, *128*, 1339–1351. [[CrossRef](#)]
37. Li, Y.; Zhao, J.; Li, C.; Wei, C.; Zhang, Y.; Guo, R.; Leng, Y.; Jiang, H. Cadmium and clay mineral analysis of late Pliocene–Pleistocene deposits from Jiangnan Basin, central China: Implications for sedimentary provenance and evolution of the Yangtze River. *Quat. Int.* **2021**, *598*, 1–14. [[CrossRef](#)]
38. Sun, X.; Tian, Y.; Kuiper, K.F.; Li, C.A.; Zhang, Z.; Wijbrans, J.R. No Yangtze River Prior to the Late Miocene: Evidence From Detrital Muscovite and K-Feldspar $^{40}\text{Ar}/^{39}\text{Ar}$. *Geophys. Res. Lett.* **2021**, *48*, e2020GL089903. [[CrossRef](#)]
39. Wang, K.; Shi, X.; Yao, Z.; Liu, J.; Liu, J.; Xu, T. Heavy-mineral-based provenance and environment analysis of a Pliocene series marking a prominent transgression in the south Yellow Sea. *Sediment. Geol.* **2019**, *382*, 25–35. [[CrossRef](#)]
40. Zhang, C.; Li, Z.; Chen, Q.; Dong, S.; Yu, X.; Yu, Q. Provenance of eolian sands in the Ulan Buh Desert, northwestern China, revealed by heavy mineral assemblages. *Catena* **2020**, *193*, 104624. [[CrossRef](#)]
41. Garzanti, E.; Liang, W.; Andò, S.; Clift, P.D.; Resentini, A.; Vermeesch, P.; Vezzoli, G. Provenance of Thal Desert sand: Focused erosion in the western Himalayan syntaxis and foreland-basin deposition driven by latest Quaternary climate change. *Earth-Sci. Rev.* **2020**, *207*, 103220. [[CrossRef](#)]
42. Xie, Y.; Kang, C.; Chi, Y.; Wu, P.; Wei, Z.; Wang, J.; Sun, L. Reversal of the middle-upper Songhua River in the late Early Pleistocene, Northeast China. *Geomorphology* **2020**, *369*, 107373. [[CrossRef](#)]